Journal of Marine Systems 132 (2014) 116–129

Contents lists available at ScienceDirect

Journal of Marine Systems

journal homepage: www.elsevier.com/locate/jmarsys

Springs–neaps cycles in daily total seabed light: Daylength-induced changes

E.M. Roberts *, D.G. Bowers, A.J. Davies

School of Ocean Sciences, Bangor University, Menai Bridge, Anglesey LL59 5AB, UK

ARTICLE INFO

Article history:
Received 20 September 2013
Received in revised form 19 January 2014
Accepted 22 January 2014
Available online 31 January 2014

Keywords:
Light
Tides
Algae
Growth
Photosynthesis
UK
North Wales
Menai Strait
France
Brittany
Bay of Brest

ABSTRACT

In shallow, tidal seas, daily total seabed light is determined largely by the interaction of the solar elevation cycle, the tidal cycle in water depth, and any temporal variability in turbidity. Since tidal range, times of low water, and often turbidity vary in regular ways over the springs–neaps cycle, daily total seabed light exhibits cycles of the same periodicity. Corresponding cycles are likely to be induced in the daily total primary production of benthic algae and plants, particularly those light-limited specimens occupying the lower reaches of a sub-tidal population. Consequently, this effect is an important control on the growth patterns, depth distribution and survival of, for example, macroalgal forests and seagrass meadows.

Seasonal changes in daylength exert an important additional control on these cycles, as they alter the fraction of the tidal and turbidity cycles occurring within daylight hours. Bowers et al. (1997) modelled this phenomenon numerically and predicted that for a site with low water at about midday and midnight at neaps tides, 6 am and 6 pm at springs, daily total seabed light peaks at neaps in winter, but the 'sense' of the cycle 'switches' so that it peaks at springs in summer — the longer daylength permits the morning and evening low water springs to contribute substantially to the daily total. Observations for such a site in North Wales (UK), presented in this paper, show that no such 'switch' occurs, and neaps tides host the largest daily totals throughout the year. The predicted 'switch' is not observed because turbidity increases generally at spring tides, and specifically at low water springs, both of which were not accounted for in the model. Observations at a second site in Brittany (France), diametrically opposite in terms of the times of low water at neaps and at springs, indicate a peak at springs throughout the year.

Analytical tools are developed to calculate the percentage of daily total sea surface irradiance reaching the bed at a site of interest on any given day, and to determine the sense of any springs–neaps cycle thereof for a given season. The conditions required for a 'switch' are explored graphically, resulting in the identification of criteria (and a useful parameter) for predicting their occurrence. Consequences for the growth patterns, depth limits and long-term survival of benthic algae and plants are discussed.

1. Introduction

Light is of primary importance to most biological communities as it provides the energy required for photosynthesis. Ambient light fields are rarely spatially homogenous and almost always vary in time. In marine environments, the ebb and flood of the tide, changes in water clarity, variable sea surface reflectance, and wave-lensing effects combine to increase the variability in the quantity and quality of light reaching benthic algae or plants far beyond that at Earth's surface, as experienced by terrestrial ecosystems (Dring, 1992; Kirk, 1994; Lobban and Harrison, 1997).

High temporal variability in seabed light means that benthic algae and plants experience periods of sufficient and insufficient light over a range of timescales (Anthony et al., 2004). Whilst they are able to store photosynthate, and thus survive extended (but largely unknown) periods of insufficient light (Vant et al., 1986), the growth and survival of an alga or plant ultimately depend upon its ability to maintain a positive energy balance in the longer term (Dennison, 1987; Duarte, 1991). This means that it must receive sufficient light to permit net photosynthesis frequently enough and for sufficient duration to offset periods of lesser light availability and net respiration. It follows that any regular temporal patterns in light availability, such as those imposed by the tide (Bowers et al., 1997; Dring, 1987), are highly important in regulating the growth, depth distribution and long-term survival of benthic algae and plants.

The amount of light incident upon the sea surface at a point in time is governed by the solar elevation (a function of time of day, time of year, and latitude) and the nature of any cloud cover. Some incident light is reflected at the air–sea boundary. If solar elevation is low and the water's surface is very smooth the reflected fraction can be large

* Corresponding author.
E-mail addresses: ospc4c@bangor.ac.uk (E.M. Roberts), oss063@bangor.ac.uk (D.G. Bowers), andrew.j.davies@bangor.ac.uk (A.J. Davies).

http://dx.doi.org/10.1016/j.jmarsys.2014.01.009

(Kirk, 1994). However, under most conditions the majority of incident light penetrates into the water column. There, it is scattered and absorbed such that it is often greatly attenuated by the time it reaches the seabed. The degree of attenuation is determined by the water depth and the clarity, or conversely the turbidity, of the water. In a shallow, tidal sea, therefore, temporal patterns in light at the seabed are largely governed by the interaction of three cycles: the solar elevation cycle; the tidal cycle in water depth; and any cyclical behaviour in turbidity.

Springs–neaps modulations are present in tidal and turbidity cycles at sites with appreciable lunar semi-diurnal (M_2) and solar semi-diurnal (S_2) tidal constituents. The tidal range grows (spring tides) and shrinks (neaps tides) with a 14.79 day periodicity, as the tide generating forces of the moon and the sun are aligned or anti-aligned. Furthermore, the times of low water advance by about 50 min each day over the springs–neaps cycle, as the period of the larger amplitude M_2 constituent is 12 h 25 min. Temporal patterns in instantaneous seabed irradiance will, therefore, evolve from day to day as the springs–neaps cycle progresses. Since daily total seabed irradiance is given by the area beneath these instantaneous irradiance curves, a corresponding springs–neaps cycle might be expected in the daily totals also. These cycles are the subject of this paper. Their importance lies in their potential ability to induce similar cycles in daily total benthic primary production, particularly of those light-limited plants and algae occupying the lower reaches of a sub-tidal population.

The exact variations in tidal range and turbidity over the springs–neaps cycle are (locally) exclusive to a particular site. Furthermore, the times of low water at different phases of the springs–neaps cycle are also site-specific; the times of low water at springs and neaps, for example, can be understood to be determined by the phase of the S_2 tide at that site (in this paper, expressed as the phase lag, in degrees, of the S_2 tidal constituent behind the corresponding constituent of the equilibrium tide at Greenwich) (Pingree and Griffiths, 1981). Thus, the form of any springs–neaps pattern in daily total seabed irradiance will be highly site-specific. It will not, however, be constant over time. Seasonal changes in daylength exert an important additional control on the patterns, as they alter the fraction of the tidal water depth (and turbidity) cycles occurring within daylight hours. This additional control is the primary focus of the current work.

The importance of the tide as a control on seabed irradiance has been noted by several authors (Anthony et al., 2004; Bowers and Brubaker, 2004, 2010; Carter and Rybicki, 1990; Gévaert et al., 2002, 2003; Koch and Beer, 1996; Pilgrim and Millward, 1989; Topliss et al., 1980). Regular changes in instantaneous and daily total seabed irradiance over the springs–neaps cycle have been explored theoretically by Dring (1987) and by Bowers et al. (1997). Observations of this phenomenon have also been reported: for winter in the Irish Sea by Topliss (1977); and for autumn and winter in the southern North Sea by Dring and Lüning (1994).

Bowers et al. (1997) modelled the springs–neaps cycle in daily total seabed irradiance for a site in North Wales (UK) with an S_2 phase of about 0°. Such a site always has low waters occurring at about 6 am and 6 pm (GMT) at spring tides; they will have advanced incrementally to about midday and midnight by neaps, seven days later. Interestingly, they predicted a 'switch' would occur in the 'sense' of the cycle; it would peak at neaps, or be *neaps-dominated*, in winter, owing to the low water of neaps tides occurring at midday. However, as the daylength increases with the arrival of summer, the morning and evening low waters of spring tides would contribute sufficiently to the daily total for it to exceed that at neaps and for the cycle to become *springs-dominated*. The turbidity was treated as constant over time in this numerical model, which is unlikely to be the case, and so it is unclear whether this switch occurs in reality.

In this paper, winter and summer observations of seabed irradiance are presented for the study site modelled in Bowers et al. (1997). The observations are used to test the aforementioned prediction of a switch. We investigate how the original prediction is affected by efforts to model variation in turbidity appropriately. Finally, analytical equations are developed for calculating two parameters at sites of interest: the percentage of daily total sea surface irradiance reaching the bed on any given day, P; and the 'springs–neaps dominance ratio', $D_{S/N}$ — a ratio devised to indicate the 'sense' of the cycle (i.e., springs- or neaps-dominated) for a given time of year. Both tools offer practical means of probing springs–neaps cycles in P, and they can be applied in winter and summer to identify, or rule out, a switch. However, we finish the paper by offering some graphical tools and mathematical criteria for identifying the possibility of such a switch more easily.

2. Materials and methods

2.1. Site description

Two study sites feature in this paper. The focus is on Menai Strait (North Wales, UK) data throughout. Data from the Bay of Brest (Brittany, France) are included to provide an additional test of the analytical tools presented.

2.1.1. Menai Strait, North Wales

The Menai Strait (Fig. 1) is a narrow, shallow sea strait separating the Isle of Anglesey from the North Wales mainland. It occupies a composite valley, which was submerged following deglaciation (Embleton, 1964). It is orientated southwest to northeast, has a minimum width of about 300 m, a maximum width of about 2 km, and a length of 20 km.

The depth of the strait below Lowest Astronomical Tide (LAT) varies from a maximum of 22 m, just to the northeast of the mooring, to a minimum of 1–2 m, at the southwest end, where a sandy sill exists near Caernarvon (Harvey, 1968). Irregular bed topography makes the identification of a single representative depth difficult. However, a mean depth estimate in the region 10–15 m is sensible and a value of 13 m was used for modelling purposes by Bowers (2003).

The dynamics of the water flow in the strait are dominated by tidal forcing (Kratzer et al., 2003). The average tidal range is 6.5 m at spring tides and 3.5 m at neaps tides (Buchan et al., 1967; Harvey, 1968), and strong tides are characteristic; the mean tidal current is 0.7 m s^{-1}, though currents over 1 m s^{-1} occur at spring tides (Bowers, 2003). Consequently, the water column remains vertically mixed throughout the year, with little difference between surface and bottom water in terms of temperature, salinity and suspended particulate matter (SPM) (Buchan et al., 1967).

The combination of a large tidal excursion (14 km at springs) relative to the length of the strait and a tide-induced residual flow to the southwest (Harvey, 1968) ensures that the strait is well flushed with water from the Irish Sea. Freshwater discharge into the strait (predominantly by the Ogwen and Seiont Rivers) is small compared with both the tidal prism and the residual flow; the salinity is typically in the range 32–34 (Buchan et al., 1967) — much like that of the adjacent regions of the Irish Sea.

Other than at the sandy, southwest end, the bed is rocky and scoured at the narrow, turbulent sections (which typically host steep, rocky shoals) and thick mud is deposited near the inner banks of some bends and in embayments, where the tidal scour is relatively weak (Buchan et al., 1967). At the site of our mooring (53°12.52′N 4°12.18′W), the bed is of compacted mud and boulders, and is sufficiently level for the deployment of a bed frame hosting instrumentation.

The water flowing through the Menai Strait usually carries a heavy load of SPM (Buchan et al., 1967). Optically, therefore, light attenuation is strongly influenced by this suspended material, but it is also influenced by coloured dissolved organic matter (CDOM) and, intermittently, phytoplankton blooms.

The phase of the S_2 tide at the Menai Strait is approximately 0° (referenced to Greenwich) (Pingree and Griffiths, 1981). Consequently, high water spring tides occur at midday and midnight (GMT). At neaps tides, it is the low waters that occur at these times.

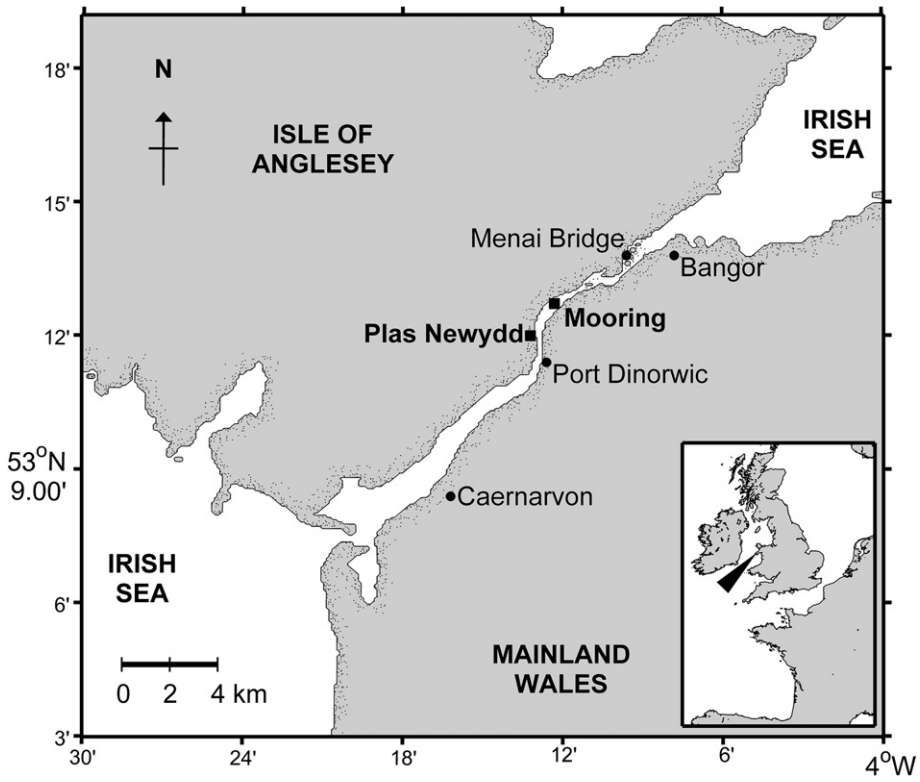

Fig. 1. The Menai Strait study site. Black squares (■) represent the positions of deployed instrumentation: the bed frame mooring between Menai Bridge and Port Dinorwic; and the roof top sensor at Plas Newydd.

2.1.2. Bay of Brest, Brittany

The Bay of Brest is a semi-enclosed coastal area (180 km^2) located at the western extremity of the Brittany Peninsula. It is connected to the adjacent Iroise Sea by a narrow strait, which is 1.8 km wide and has a maximum depth below LAT of about 50 m. The bay itself is somewhat shallower, having a mean depth of 10 m and wide shoals; only 15% of the total area is deeper than 20 m (Monbet and Bassoullet, 1989) and 50% is less than 5 m deep (Thouzeau et al., 2000).

Like the Menai Strait, the hydrodynamics are dominated by tidal forcing. The average tidal range is 4.2 m, and a range of 7.5 m is reached at large spring tides (Monbet and Bassoullet, 1989). The consequence is that large exchanges of water occur through the strait, with tidal currents there reaching speeds of up to 2 m s^{-1} (Salomon and Breton, 1991). The tidal action also results in a large clockwise residual water circulation in the bay (Salomon and Breton, 1991).

It is possible to distinguish three regions within the Bay of Brest: a northern basin; a southern basin; and a central region, connecting the two basins with the strait. 80% of the freshwater input to the bay is provided by two rivers — the Élorn provides 15% of the freshwater input and drains into the northern basin, and the Aulne provides 65% and drains into the southern basin (Le Pape, 1997). These inputs are almost negligible compared to the exchange of water with the Iroise Sea; the total annual river discharge is only equivalent to the volume exchanged with the Iroise Sea during one semi-diurnal tidal period (Monbet and Bassoullet, 1989). All three regions of the bay are thus typically well mixed (Delmas and Tréguer, 1983) by the tide, with salinity values in the range 32 to 35.5 (Delmas, 1981).

There is evidence of quasi-permanent haline stratification in the estuaries of the Élorn (L'Yavanc, 1984) and the Aulne (Bassoullet, 1979), which intensifies (and extends considerable distances into the bay) with river flow and diminishes with tidal range/stronger vertical mixing (Le Pape, 1997). Heavy rainfall did occur during a December deployment in the bay. However, it corresponded with extremely high wind velocities (Storm 'Joachim') and a marked haline stratification is unlikely to have been sustained for any appreciable period at our mooring site (48°17.55′N 4°26.96′W) in the southern basin, given its distance from the Aulne Estuary and the prevalent wind conditions and sea state.

The Bay of Brest is more directly connected to the oceanic waters of the Atlantic than the Menai Strait, which is buffered by the Irish and Celtic Seas. Its water is accordingly less turbid but can still be considered coastal in optical type, light attenuation being influenced strongly by SPM, CDOM and phytoplankton.

Of primary importance to the present study, the phase of the S_2 tide at the Bay of Brest is approximately 180° (referenced to Greenwich), that is, directly out of phase with that at the Menai Strait. Thus, the opposite scenario prevails — low water spring tides occur at around midday and midnight, whereas at neaps tides high waters occur at these times.

2.2. Overview of the fieldwork campaign

Both study sites were visited in summer and winter (Menai Strait: January; June; and August 2011. Bay of Brest: July; and December 2011). The objective was to obtain time series measurements of seabed and sea surface irradiance, as well as water depth above the submerged instrument, for entire springs–neaps cycles under different conditions of S_2 phase (i.e., location) and daylength (i.e., season). Deployment duration ranged from 2 to 4 weeks, the precise length being dictated by the onset of biofilm development or by the weather and hydrodynamic conditions at the proposed date of deployment or recovery.

2.3. Measurement of seabed and sea surface irradiance

Seabed irradiance was measured using an internally-logging irradiance sensor, deployed in a stainless steel bed frame (the positions of the bed frame are indicated in Figs. 1 and 2). The sensor's vertical position was a constant 1.5 m above the seabed; its depth below

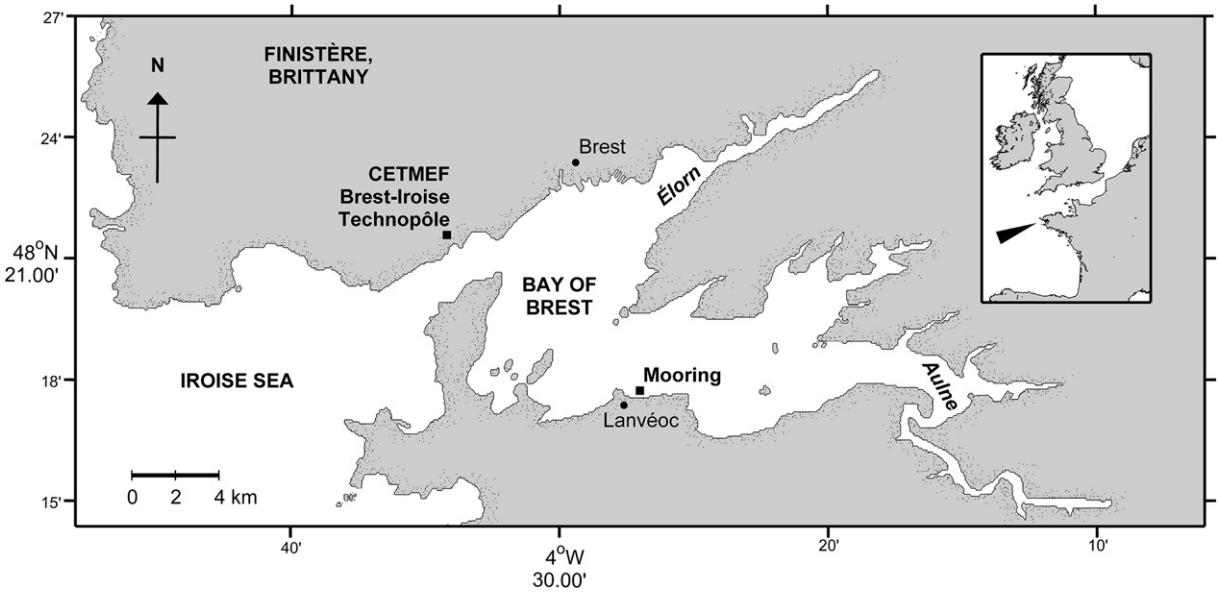

Fig. 2. The Bay of Brest study site. Black squares (■) represent the positions of deployed instrumentation: the bed frame mooring near Lanvéoc; and the roof top sensor at CETMEF.

mean sea level varied slightly from one deployment to another owing to differences in weather and hydrodynamic conditions when attempting to deploy the frame on suitable substrate with a flat topography. At the Menai Strait, this variation was minimal and the mean depth of the instrument was in the range 3.8 m to 4.4 m for each of the three deployments. At the Bay of Brest, deployment difficulties resulted in a mean depth of 4 m in the winter and 5.5 m in the summer. The sensor remained submerged at all phases of the tide throughout every deployment.

For practical reasons, sea surface irradiance was measured above the surface, rather than at or just below it; an identical irradiance sensor was positioned on the roof of a nearby building for the duration of each deployment. At the Menai Strait study site, this was a National Trust property on the banks of the strait, known as Plas Newydd (53°12.15′N 4°12.96′W, see Fig. 1). In Brittany, the Centre d'Études Techniques Maritimes et Fluviales (CETMEF), at the Brest-Iroise Technopôle, provided accessible roofspace (48°21.52′N 4°34.01′W, Fig. 2). In both cases, care was taken to ensure that the sensor was not over-shadowed by adjacent buildings or trees. The sensor bracket was modified to incorporate spikes as a deterrent to birds.

The irradiance sensors deployed were of the type MDS-MkV/L, manufactured by JFE Advantech Co. Ltd. (Kobe, Japan). They measure quantum *scalar irradiance* – the integral of the radiance distribution at a point, over all directions about that point (Kirk, 1994) – in the photosynthetically active radiation (PAR) band (approximately 400–700 nm).

During each deployment, the surface and submerged sensors were synchronised and set to measure irradiance every 2 min. The simultaneous time series were later used, together with a record of water depth (see Section 2.4), to determine a time series of the diffuse attenuation coefficient of PAR, k_{PAR}, a measure of turbidity (see Section 3.2). Two points should be noted here. Firstly, the surface and submerged sensors were separated by approximately 2 km at the Menai Strait and 12 km at the Bay of Brest. Differences in surface irradiance at the positions of the two sensors, particularly owing to cloud effects, have the potential to produce spurious short-term variability in the derived k_{PAR} time series. Secondly, we use k_{PAR} in this paper to represent the vertical attenuation coefficient of *scalar irradiance*, since this is the parameter measured by our instruments. An analogously defined attenuation coefficient of *irradiance* (were this to be measured instead) would be somewhat different in value, though with the most commonly measured parameter being downward irradiance the difference would typically be small (Kirk, 1994).

Each instrument was calibrated by the manufacturer against an LI-189 (LI-COR Biotechnology, Lincoln, Nebraska, USA) reference sensor, using a halogen light source. The manufacturers claim an accuracy of ±4% (Full Scale) and provide graphical representations of the instrument's angular and spectral response. The resolution is 1 μmol quanta m^{-2} s^{-1}.

The two instruments were intercalibrated 'in the field' (as opposed to in a laboratory), under natural light varying in intensity with the solar elevation cycle and with cloud cover. Data from intercalibrations performed pre- and post-fieldwork campaign were combined to produce a single, linear intercalibration equation, which was used to correct observations for differences in instrument sensitivities. It should be noted that these corrections were small to negligible (always less than, and often much less than, 15%) and no substantial changes in relative sensitivities occurred over the course of the fieldwork campaign.

As the sensors were calibrated in air, any underwater readings must be multiplied by an appropriate factor, or 'immersion coefficient' (in this case, approximately 1.7), to account for the so called 'immersion effect' (see Kirk, 1994). This correction is included in the sensors' firmware as a matter of course; it is assumed they will be used underwater. In the present study, however, one sensor was used in water and the other in air. It was therefore necessary to reverse this correction for data obtained with the surface irradiance sensor.

The 'dark current' irradiance reading (see Topliss et al., 1980) was typically 1 μmol quanta m^{-2} s^{-1} in magnitude and this was deducted from every irradiance measurement in each record before further analysis.

2.4. Measurement of water depth above the seabed irradiance sensor

A DST Centi TD (temperature-depth) sensor (Star Oddi Ltd., Reykjavík, Iceland) was fixed to the bed frame at the height of the irradiance sensor. This provided a simultaneous record of the depth of the overlying, tidally-varying, water column. The depth sensor was also internally logging; its clock was synchronised with those of the irradiance sensors, and it measured depth at the same frequency (i.e., every 2 min) with a resolution of 1 cm and an accuracy of ±10 cm.

The 'depth' sensor actually records the summative pressure from the overlying head of water and the atmosphere. A typical, constant atmospheric pressure is automatically deducted from each measurement to isolate the pressure resulting from the head of water alone. A correction for variations in atmospheric pressure (i.e., departures from the typical value used) was made possible by the interpolation of hourly atmospheric pressure records to match the measurement frequency. Atmospheric pressure records were obtained from the METAR reports generated by the meteorological stations at nearby military airbases: RAF Valley Airbase (53°15.01′N 4°32.35′W) in the case of the Menai Strait study site; Lanvéoc-Poulmic Airbase (48°16.93′N 4°26.50′W) in the case of the Bay of Brest.

Corrected hydrostatic pressures were converted to water depths above the instrument by dividing by the product of water density and acceleration due to gravity. Water density is a function of temperature, salinity and pressure, and was calculated according to the International Equation of State of sea water (IES-80) using measured temperatures – the DST Centi measures temperature as a secondary parameter – and pressures, and an estimate of salinity (34 is appropriate for both sites). Acceleration due to gravity was determined, using the International Gravity Formula (IGF), to be the same (to 2 decimal places) at both study sites.

2.5. Biofouling

Biofouling of the submerged optical instrument was a serious concern and occurred in three distinct forms.

Firstly, dislodged benthic macroalgae became entangled with the bed frame and mooring. The typically more buoyant Wracks collected around the buoy line (horizontally displaced some 30 m from the optical instrument) and the somewhat less buoyant species (e.g., Kelps) became entangled with the pyramidal base of the bed frame. 'Rafts' of seaweed were removed from the buoy line every few days and did not grow very large during the interval. Seaweed entanglement with the bed frame appeared, upon recovery, to occur well below the height of the irradiance sensor, probably owing to the fact that the protective framework surrounding the instruments was cylindrical in construction (with the cylinder's axis aligned vertically) in order to deflect macroalgae. There is no evidence in the irradiance records of prolonged shading or coverage of the instrument's irradiance collector.

Secondly, a gradual 'filming' of the instrument's collector was observed; a green-brown biofilm developed on its polyoxymethylene surface. This occurred in the summer months and became apparent only after 2–3 weeks of underwater deployment. A regular cleaning routine would have involved frame recovery and re-deployment, and was thus considered too disruptive; consistency of the frame's position and mean depth, and thus the integrity of the irradiance time series records, were of utmost importance in the current study. Mathematical correction for such 'filming' could not be achieved with any degree of confidence and, ultimately, this phenomenon lead to the curtailment of affected records (post-recovery) at about 2 weeks in length.

Finally, several species of benthic fauna adopted the frame as new habitat. Examination of the bed frame upon recovery indicated that the transit of very small gastropods over the irradiance collector was a possibility. Such an event is likely to have been infrequent, brief and of negligible consequence. The sensor was completely unaffected by the settling of sessile fauna.

3. Results

3.1. Menai Strait observations: winter and summer

Figs. 3 and 4 show a winter and a summer data set, respectively, from the Menai Strait. In both figures, three panels are present: an upper panel (a) displays sea surface irradiance, I_0; a middle panel (b) shows seabed irradiance, I_B, and the associated tidal variation in water depth, z; and a lower panel (c) gives the percentage of daily total sea surface irradiance received by the seabed, P. We define P more formally as

$$P = \frac{<I_B>}{<I_0>} \times 100, \quad (1)$$

where angular brackets denote daily totals of the enclosed parameters. Daily totals were determined by numerical integration (using the Trapezium Rule) of the appropriate irradiance time series with respect to time.

Evidence of the different controls on seabed irradiance is abundant in both data sets. The most important controls are highlighted here such that the reader may gain contextual understanding.

Surface irradiance control is apparent when the seabed irradiance curve closely resembles that at the sea surface. Cloud-free days, for example the 28th and 29th January (Fig. 3(a) and (b)), have smooth, Gaussian-shaped surface irradiance curves, owing to the variation in

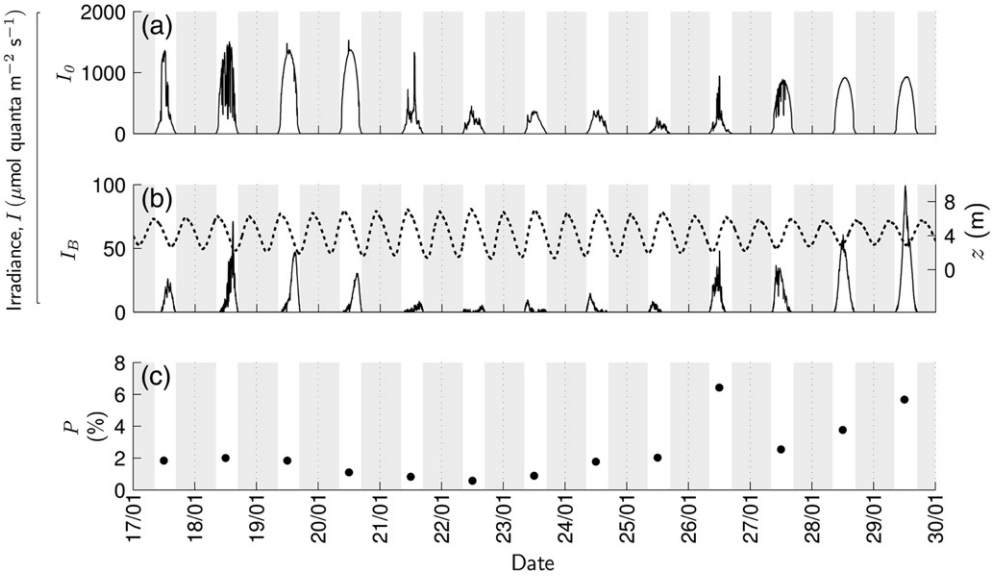

Fig. 3. Winter (January 2011) time series from the Menai Strait: (a) sea surface irradiance, I_0; (b) seabed irradiance, I_B (solid line), and water depth, z (dashed line); and (c) the percentage of daily total sea surface irradiance that is received by the seabed on each day, P. Areas shaded grey represent periods of darkness or twilight occurring at night.

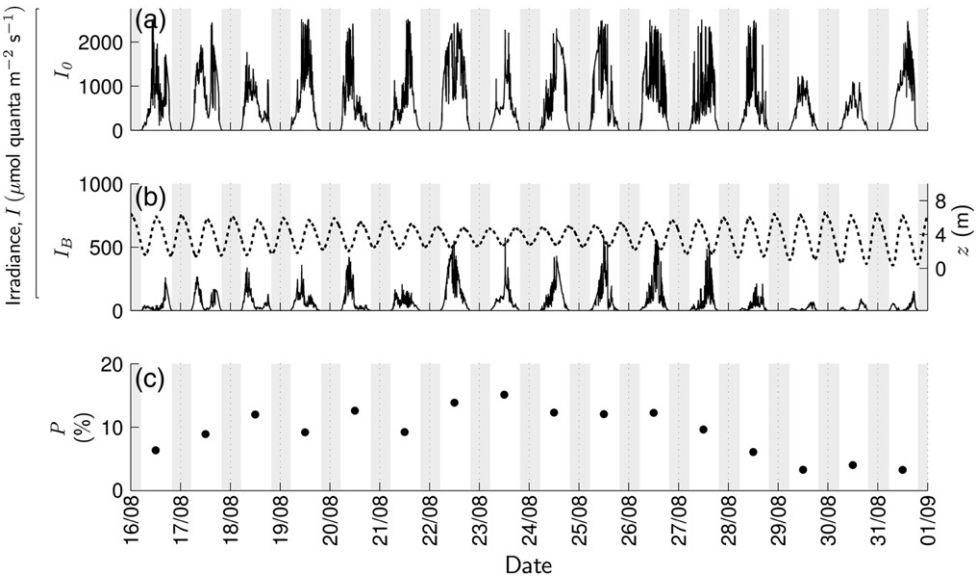

Fig. 4. Summer (August 2011) time series from the Menai Strait: (a) sea surface irradiance, I_0; (b) seabed irradiance, I_B (solid line), and water depth, z (dashed line); and (c) the percentage of daily total sea surface irradiance that is received by the seabed on each day, P. Areas shaded grey represent periods of darkness or twilight occurring at night.

solar elevation over the day, and the seabed irradiance curve is correspondingly smooth. Cloudy days have irregular, jagged surface irradiance curves, and the seabed irradiance exhibits a distinctly similar pattern. A good example is the 23rd August (Fig. 4(a) and (b)).

Tidally-varying water depth as a control is characterised by peaks in seabed irradiance that correspond approximately to the times of low water, as the depth of the attenuating medium is reduced at these times. The 'two peak' pattern is perhaps the most compelling evidence for tidal control and occurs when two low waters occur within, or nearly within, one 'daytime'. The clearest examples are found at spring tides during summer (see Fig. 4), and the phenomenon is addressed analytically by Bowers and Brubaker (2004).

Tidal variability in turbidity, on semi-diurnal and springs–neaps timescales, occurred during both deployments and, though not clearly apparent in Figs. 3 and 4, was an important control on seabed irradiance. It is explored in greater depth in the next Section (3.2).

Seasonal control of sea surface (and thus seabed) irradiance by the annual cycle in solar declination – the angle through which the northern hemisphere (in this case) is tilted towards or away from the sun (Kirk, 1994) – is demonstrated by longer daylengths and higher peak irradiances in summer (Fig. 4) than in winter (Fig. 3).

In this paper, we are interested in P, and any springs–neaps cycles thereof. Panel (c) in Figs. 3 and 4 is therefore of primary interest. The percentages reflect the net effect of all the controls described above, with their relatively different levels of importance, on seabed irradiance over a day. Springs–neaps cycles in the percentages are generated by cycles of this periodicity in the tidal controls on seabed irradiance (i.e., water depth and turbidity). Noise in the generally smooth springs–neaps cycles in P is most often the result of the variable nature and irregular timing of cloud cover, relative to the more regular variations in the tidal controls. The best illustrative example of this occurs on the 26th January (Fig. 3). On this day, a brief cloud-free period occurring in the late morning is coincident with low to mid-tide and a cloudy afternoon is coincident with high tide — a chance scenario that serves to enhance the calculated percentage on that day.

In both Figs. 3 and 4, the largest percentages occur at neaps tides and the smallest at springs. A springs–neaps cycle is apparent, despite noise, and has a larger mean value and amplitude in summer than in winter. Crucially, and in disagreement with the earlier work of Bowers et al. (1997), *the sense of the cycle does not appear to change from winter to summer*. That is to say, for the Menai Strait, *neap tides host the largest percentages throughout the year* — the cycle is always neaps-dominated.

3.2. Exploring temporal patterns in turbidity

An explanation must be sought as to why the sense of the springs–neaps cycle in P at the Menai Strait does not 'switch' with the arrival of the longer summer daylengths, as predicted by the numerical model of Bowers et al. (1997). To this end, we test the simplifying assumption, employed in the Bowers model, that turbidity, represented by the diffuse attenuation coefficient of PAR or k_{PAR}, is constant over time.

Fig. 5 shows a time series of instantaneous k_{PAR} (Panel (b)) and daily mean values (Panel (c)), denoted by an overbar (i.e., $\overline{k}_{PAR}$). The former time series was derived from the simultaneous records of I_0, I_B and z, by solving the Lambert–Beer Law (Eq. (3)) for k_{PAR}. Daily means were determined by averaging the instantaneous k_{PAR} values for each day. It is immediately apparent that k_{PAR} is not constant in time for the Menai Strait; k_{PAR} varies on tidal cycle timescales and $\overline{k}_{PAR}$ varies from day to day, in a regular way, over the springs–neaps cycle.

It is possible to hypothesise that two separate physical mechanisms are at work here. First, daily mean current speeds increase at spring tides and the additional energy in the system might be expected to resuspend more bed material and to elevate $\overline{k}_{PAR}$ generally at these times (Fig. 6). Second, a shallow water effect may exist such that, at low water, wave or tidal resuspension of sediments may be capable of increasing the turbidity of the entire water column (Fig. 7).

From Fig. 6, it can be seen that a power law (power 3) describes approximately the relationship between $\overline{k}_{PAR}$ and daily mean tidal range, $\overline{R}$. Power 3 was selected on the basis that the turbulent kinetic energy available for sediment resuspension, a major control on turbidity, is proportional to the cube of current speed (Bowers, 2003). As daily mean current speed in the strait is linearly proportional to $\overline{R}$ (MacDonald, R., 2013, personal communication, 11 March), it follows that we might try to express $\overline{k}_{PAR}$ as some function of $\overline{R}^3$. In fact, the inclusion of an offset (i.e., $(\overline{R}-2)^3$) is preferable, so that $\overline{k}_{PAR}$ grows from a minimum, or background level, at neaps with the *increment* in tidal range (from that at neaps), cubed, rather than with *absolute* tidal range cubed. In this case, $\overline{R}$ is in metres and the offset value of 2 represents approximately the tidal range at neaps (i.e., 2 m). In addition to this daily

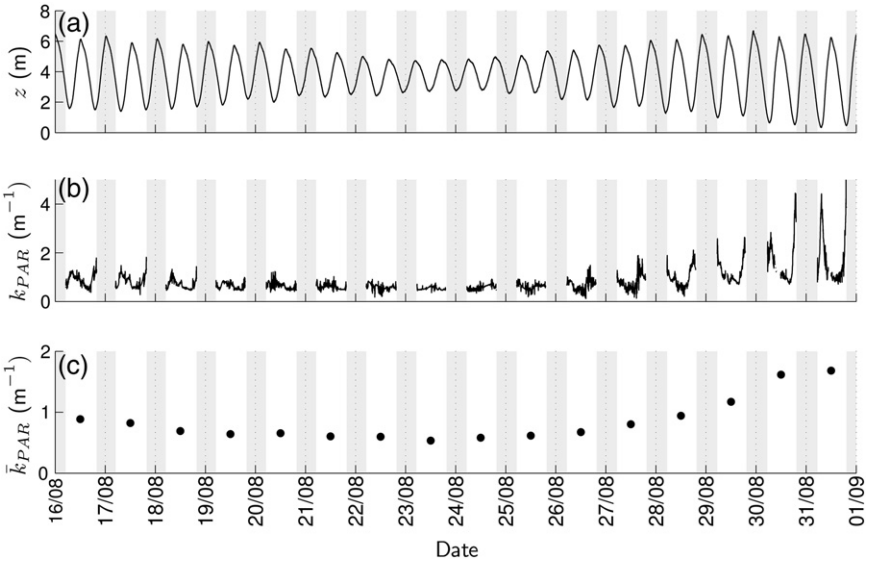

Fig. 5. Summer (August 2011) time series from the Menai Strait: (a) water depth, z; (b) instantaneous diffuse attenuation coefficient of PAR, k_{PAR}; and (c) daily mean diffuse attenuation coefficient of PAR, $\bar{k}_{PAR}$. Note the apparent springs–neaps cycle in $\bar{k}_{PAR}$, indicating a dependence on tidal range, and the oscillation of instantaneous k_{PAR} with water depth — maxima coinciding with low water and minima at, or just after, high water.

mean ($\bar{k}_{PAR}$) behaviour, instantaneous k_{PAR} may be said to vary in inverse proportion to the water depth (see Fig. 7).

The variability in k_{PAR} may be quantified simply by first linearising the August 2011 data – transforming $\bar{R}$ and z according to the understanding gained from the curves in Figs. 6 and 7 – and then by performing a multiple linear regression. We arrive at an equation of the following form:

$$k_{PAR} = A + B(\bar{R}-2)^3 + C\left(\frac{1}{z} - \frac{1}{z_0}\right), \tag{2}$$

where: A, B and C are constants determined by the regression to be $(0.575 \pm 0.004)\text{m}^{-1}$, $(0.0088 \pm 0.0002)\text{m}^{-4}$ and (1.17 ± 0.01), respectively; k_{PAR}, $\bar{R}$ and z are as defined previously; and z_0 is the mean water depth. The coefficient of determination, R^2, for the fit is 0.79.

An equation of this form represents a sensible physical understanding of k_{PAR} variability over time. The first two terms provide a daily mean k_{PAR} value governed by the tidal range on a given day; the third term permits instantaneous k_{PAR} to oscillate about this daily mean with changes in water depth. Inclusion of the $1/z_0$ term means that k_{PAR} is equal to its daily mean value when $z = z_0$ (i.e., at mid-tide). This is approximately true on most days and is thus a reasonable first order approximation for our purposes.

The simple approach adopted here (Eq. (2)) reproduces the patterns in the August k_{PAR} data well with a Root Mean Squared (RMS) Error of 0.22 m^{-1}. It therefore offers a semi-empirically determined means of modelling k_{PAR} temporal variability with which to update the Bowers et al. (1997) numerical model and examine the consequences.

3.3. Updating the numerical model

The numerical model employed and developed here (for the Menai Strait) is described fully in Bowers et al. (1997) but we recap briefly for completeness.

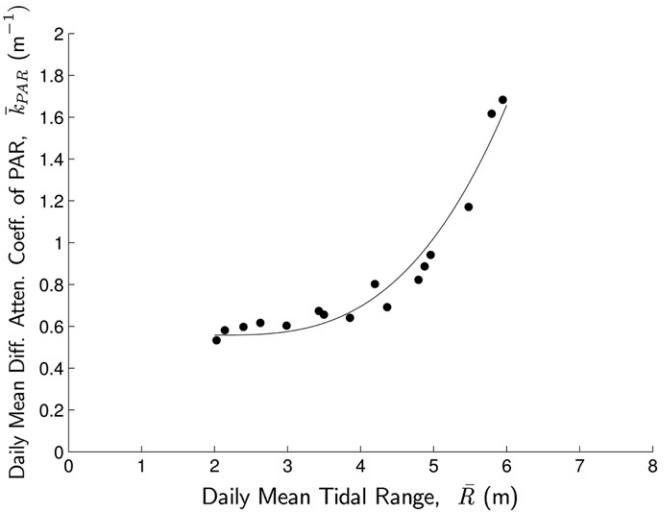

Fig. 6. Daily mean diffuse attenuation coefficient of PAR, $\bar{k}_{PAR}$, plotted against daily mean tidal range, $\bar{R}$. The data is from the summer (August 2011) Menai Strait deployment. An offset power law is displayed, for illustrative purposes only, with the general form $\bar{k}_{PAR} = p + q(\bar{R}-2)^3$, where p and q are constants.

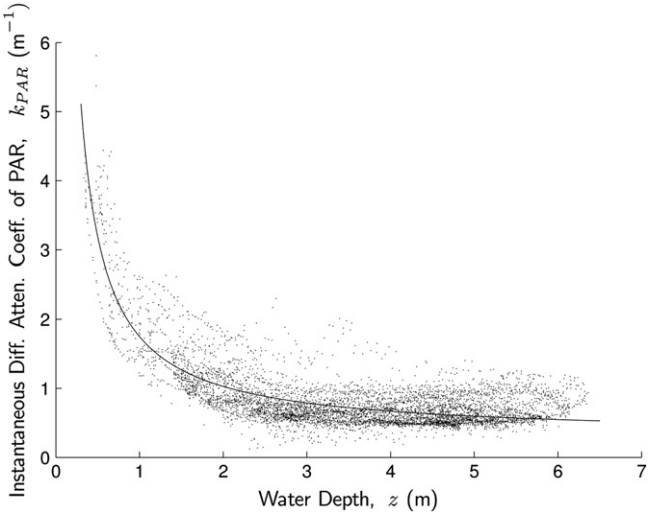

Fig. 7. Instantaneous diffuse attenuation coefficient of PAR, k_{PAR}, plotted against water depth, z. The data is from the summer (August 2011) Menai Strait deployment. A curve with the form $k_{PAR} = m + (n/z)$, where m and n are constants, is provided to illustrate the approximate nature of the relationship only.

Sea surface irradiance, $I_0(t)$, was modelled using a set of equations taken from Kirk (1994) that reproduce cloud-free conditions; they are functions of latitude, time of day and of year. Seabed irradiance, $I_B(t)$, is computed as the sea surface irradiance attenuated exponentially by the product of the diffuse attenuation coefficient of PAR, $k_{PAR}(t)$, and the water depth, $z(t)$, in accordance with the Lambert–Beer Law,

$$I_B(t) = I_0(t)\exp[-k_{PAR}(t)z(t)]. \quad (3)$$

This law typically applies to monochromatic light but also applies approximately to irradiance integrated over the entire PAR waveband (Kirk, 1994), as required here.

$z(t)$ was simulated by the sum of a lunar and a solar semi-diurnal tide, that is the M_2 and S_2 tidal constituents respectively, to produce a springs–neaps cycle. The amplitudes input for each constituent are representative of the Menai Strait (2 m for the M_2 and 1 m for the S_2). The S_2 phase was set to 0° so that high water springs (and thus low water neaps) occur at midday, as is the case in the strait. A mean water depth of 4 m was selected so that the model output is comparable with our observations, which were made at approximately this mean depth.

The principal development made in the current work was that k_{PAR} was not set to be constant in time. Instead, $k_{PAR}(t)$ was modelled using the semi-empirical Eq. (2), determined in Section 3.2. In this equation, k_{PAR} is not only a function of $z(t)$, which was modelled as outlined above, but also a function of daily mean tidal range, $\overline{R}(t)$, which we represented as varying, from day to day, cosinusoidally about an average value with the period of the springs–neaps cycle. The mean and amplitude of this cycle in $\overline{R}$ were set to 4 m and 2 m respectively to emulate the changes in tidal range occurring in our modelled water depth. An example output from the model, for an arbitrary springs–neaps cycle in mid-summer, is shown in Fig. 8 and illustrates the nature of the cycles in key parameters.

As with the original form of the model, single peaks in I_B are reproduced at neaps tides and the interesting 'two peak' pattern is seen at springs. However, the increasing k_{PAR} at springs generally and at very low waters in particular, in the updated form of the model, ensures that the peaks in I_B generated at springs are now more realistic, being lower than their counterparts at neaps.

Daily total seabed and sea surface irradiances are proportional to the area beneath the appropriate daily irradiance curves, such as those in Fig. 8(d); they are again computed by numerical integration (using the Trapezium Rule) of irradiance over time. Thus, the model can output P on any given day. Fig. 9 shows this modelled parameter over an entire year for the Menai Strait. In fact, the output for two different parameterisations of the model is displayed in the figure for comparison. The upper panel (Fig. 9(a)) shows the output if k_{PAR} is set to be constant over time, as in Bowers et al. (1997); the lower panel (Fig. 9(b)) shows the output if k_{PAR} varies according to Eq. (2).

Fig. 9 demonstrates an important result. When k_{PAR} is constant in time, a switch occurs in the sense of the springs–neaps cycle in P (Fig. 9(a)), as reported in Bowers et al. (1997). The cycle is neaps-dominated in the short days of winter because low water neaps tides occur at midday, whereas low water spring tides occur during the hours of darkness. As summer approaches, and daylength increases, low water spring tides occur within daylight hours; the daily total seabed irradiance at springs is significantly enhanced, exceeding that at neaps, and the sense of the cycle switches to springs-dominated. However, if k_{PAR} is permitted to vary in a realistic way, being generally greater during the energetic spring tides and increasing markedly at very low waters, the daily totals at springs are not sufficiently enhanced by longer summer days and no switch occurs (Fig. 9(b)). The cycle remains neaps-dominated throughout the year, in agreement with our observations.

3.4. Useful analytical and graphical tools

Benthic ecologists and optical oceanographers might be interested to learn about the patterns in P occurring at other study sites. Three main questions arise: (1) what percentage of daily total sea surface irradiance reaches the bed on a given day; (2) does a springs–neaps cycle in the percentage exist and, if so, is it springs- or neaps-dominated; and (3) is the sense of the cycle likely to switch seasonally (i.e., what are the criteria for a switch)? We present three mathematical tools that can be used to answer these questions. The tools are analytically derived, and values calculated with them should therefore be considered approximate only. Despite this, such analytical tools allow the

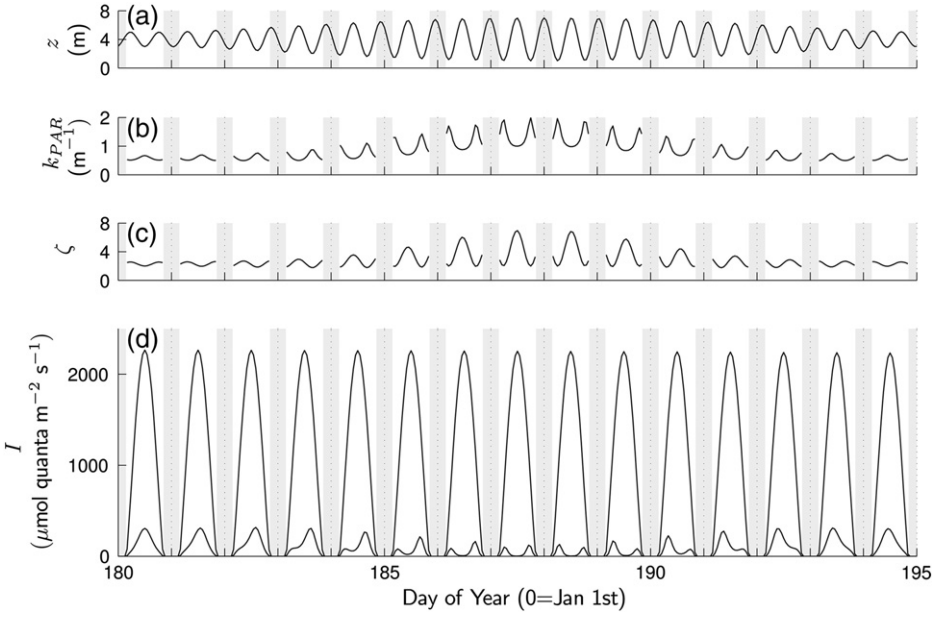

Fig. 8. Numerical model output for an arbitrary 15 day period in mid-summer at the Menai Strait study site. Panels (a) and (b) illustrate the modelled variation in water depth, z, and diffuse attenuation coefficient of PAR, k_{PAR}, respectively. Panel (c) shows the dimensionless diffuse optical depth of the water column, ζ, which is defined as the product $k_{PAR}z$. Panel (d) displays both sea surface irradiance, I_0, and seabed irradiance, I_B, which at any point in time is I_0 attenuated exponentially by ζ, in accordance with the Lambert–Beer Law. Grey-shaded areas represent night-time.

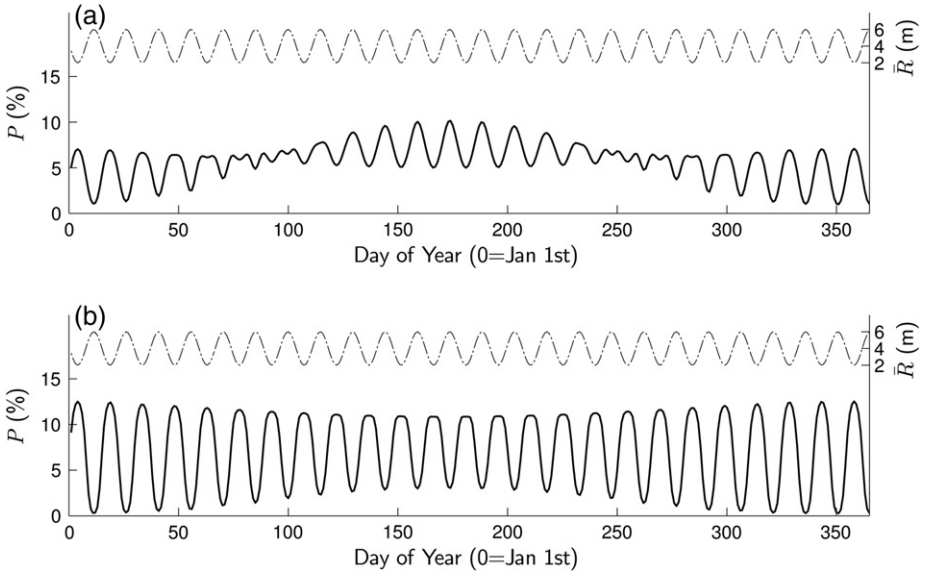

Fig. 9. Percentage of daily total sea surface irradiance received by the seabed each day, *P*, modelled over a year for the Menai Strait. Model output is presented for two parameterisations: (a) diffuse attenuation coefficient of PAR, k_{PAR}, is constant over time; and (b) k_{PAR} varies with daily mean tidal range, $\overline{R}$, and water depth, *z*, according to Eq. (2). The switch from a neaps-dominated to a springs-dominated cycle with the arrival of summer in the former parameterisation does not occur in the more physically realistic lower panel, where the cycle remains neaps-dominated throughout the year in agreement with observations. $\overline{R}$ is plotted (dash-dotted line) so that the sense of the cycles may be easily interpreted.

physical understanding we have gained thus far to be applied and tested in new locations.

3.4.1. Tool 1: percentage of <I_0> received by the seabed on a given day

In the definition of *P* given by Eq. (1) note that the numerator, <I_B>, may be determined by integrating the Lambert–Beer Law (Eq. (3)) over the hours of daylight. The denominator, <I_0>, is determined by integrating the function selected for $I_0(t)$ over the same period. Thus, we may restate *P* as

$$P = \frac{\int_{-L/2}^{L/2} I_0(t)\exp[-k_{PAR}(t)z(t)]\,dt}{\int_{-L/2}^{L/2} I_0(t)\,dt} \times 100, \quad (4)$$

where *t* is time relative to midday, *L* is the daylength (i.e., the number of daylight hours) and all other symbols are as defined previously.

An analytical form of the denominator in Eq. (4) is relatively straightforward to achieve. As in Bowers and Brubaker (2010), $I_0(t)$ is approximated as a Gaussian curve given by $I_M \exp[-(t/q)^2]$, where I_M is the maximum, or midday, surface irradiance, *t* is the time relative to midday and *q* is a parameter that sets the width of the Gaussian curve such that it approximates the daylength. Bowers and Brubaker (2004, 2010) found that $q \approx L/3$ ensures the Gaussian curve offers a reasonable fit to observations of I_0. An analytical expression for <I_0> is then determined using the definite integral of a Gaussian curve, giving $\langle I_0 \rangle = I_M q\sqrt{\pi}$.

An analytical expression for the numerator in Eq. (4) is more challenging. Since I_0, k_{PAR} and *z* are all functions of time, finding an analytical equation for <I_B> is a case of representing each of these as simple functions that combine to give an integral with a solvable form. As above, we approximate $I_0(t)$ using the equation for a Gaussian curve. A daily average diffuse attenuation coefficient of PAR, $\overline{k}_{PAR}$, is employed. This is not ideal; we have seen that k_{PAR} varies, not only from day-to-day with the springs–neaps cycle, but also on shorter timescales, for example, during the day with water depth (Section 3.2). However, the simplification is necessary to make an analytical solution possible. Typically, $z(t)$ would be represented by $z_0 - (\overline{R}/2)\cos(\omega(t - t_{lw}))$, where z_0 is the mean water depth, $\overline{R}$ is the mean or typical tidal range for the day, ω is the angular frequency of the tide (0.5 h^{-1} for a semi-diurnal tide), *t* is the time and t_{lw} is the time of low water (both relative to midday). Further simplification is required, however, and we expand the cosine term into its equivalent power series and select the first two terms only. Thus, $z(t)$ is approximated as a parabola about low water, given by $z_0 - (\overline{R}/2)\left(1 - \omega^2(t - t_{lw})^2/2\right)$. The limitations introduced by such an approximation are explored in some depth by Bowers and Brubaker (2010).

Applying the above approximations and rearranging gives an analytical equation for $I_B(t)$ as follows:

$$I_B(t) = \alpha I_M \exp[-\phi]\exp\left[-a(t - t_P)^2\right], \quad (5)$$

where

$$\alpha = \exp\left[\overline{k}_{PAR}\left((\overline{R}/2) - z_0\right)\right],$$

$$\phi = (x/(x+1))(t_{lw}/q)^2,$$

$$a = \left(1/q^2\right)(x+1),$$

$$t_p = (x/(x+1))t_{lw},$$

and

$$x = 0.25\overline{k}_{PAR}\overline{R}\omega^2 q^2.$$

I_M, α, ϕ, *a*, t_p and *x* are all constants on any given day. Consequently, Eq. (5) also has the form of a Gaussian 'pulse' of irradiance at the seabed. The pulse peaks at a value of $I_B = \alpha I_M \exp[-\phi]$ when $t = t_p$, where t_p is the time of the peak (see Bowers and Brubaker (2004) for a detailed analysis of the timing of these peaks).

The definite integral of a Gaussian curve is used again, this time to provide an analytical expression for <I_B>, giving $\langle I_B \rangle = \alpha I_M \exp[-\phi]\sqrt{\pi/a}$. In reality, two peaks in seabed irradiance may be produced if two low waters occur within (or nearly within) daylight hours.

A more general form of the expression is therefore required; $\langle I_B \rangle = \alpha I_M (\exp[-\phi_1] + \exp[-\phi_2])\sqrt{\pi/a}$ (with the subscripts 1 and 2 on ϕ relating to two low waters). This accounts for the possibility of two pulses in I_B. Note that the form of ϕ ensures low waters occurring considerably outside of daylight hours cannot contribute significantly to the daily total.

Substituting the expressions for $\langle I_B \rangle$ and $\langle I_0 \rangle$ into Eq. (1) and simplifying provides our first analytical tool, an equation for the percentage of daily total sea surface irradiance received by the bed on any day,

$$P = \frac{\alpha}{\sqrt{x+1}}(\exp[-\phi_1] + \exp[-\phi_2]) \times 100. \quad (6)$$

Fig. 10(a) shows a plot of P values predicted using Analytical Tool 1 (Eq. (6)) against observed values from the five fieldwork campaigns carried out in 2011.

3.4.2. Tool 2: springs or neaps dominance tool

The 'sense' of a springs–neaps cycle in P at a given location and time of year (i.e., springs-dominated or neaps-dominated) can be determined simply by taking the ratio of the percentage at springs, P_S, to that at neaps, P_N. We therefore use Eq. (6) to define a 'springs–neaps dominance ratio', $D_{S/N}$, as

$$D_{S/N} = \frac{P_S}{P_N} = \frac{\alpha_S}{\alpha_N}\sqrt{\frac{x_N+1}{x_S+1}}\frac{\exp\left[-\phi_{1,S}\right] + \exp\left[-\phi_{2,S}\right]}{\exp\left[-\phi_{1,N}\right] + \exp\left[-\phi_{2,N}\right]}, \quad (7)$$

where the subscripts S and N denote springs and neaps values respectively. Springs parameters are defined as $\alpha_S = \exp\left[\bar{k}_{PAR,S}((\bar{R}_S/2)-z_0)\right]$, $x_S = 0.25\bar{k}_{PAR,S}\bar{R}_S\omega^2 q^2$, $\phi_{1,S} = (x_S/(x_S+1))(t_{lw1,S}/q)^2$ and $\phi_{2,S} = (x_S/(x_S+1))(t_{lw2,S}/q)^2$, where $t_{lw1,S}$ and $t_{lw2,S}$ refer to the time, relative to midday, of the first and second low waters, respectively. Neaps parameters (i.e., α_N, x_N, $\phi_{1,N}$ and $\phi_{2,N}$) are defined identically, except that all S subscripts in the definitions above are replaced by an N.

A $D_{S/N}$ value greater than 1 indicates a springs-dominated cycle for that particular site and time of year. A $D_{S/N}$ value less than 1 indicates a neaps-dominated cycle, and a value equal to 1 indicates no discernable cycle.

Fig. 10(b) shows a plot of observed $D_{S/N}$, determined from the springs–neaps cycles in P that were apparent over five fieldwork campaigns, against $D_{S/N}$ predicted for the same sites and times of year using Analytical Tool 2 (Eq. (7)).

In this paper, we consider *either* springs *or* neaps hosting the largest P values in any cycle. Though this appears to be true for our two sites – Menai Strait and Bay of Brest represent two opposite and straightforward cases (low water neaps at midday in the former, low water springs at midday in the latter) – it is not ubiquitous. At locations with other S_2 phases, low water occurs at midday on days between springs and neaps and, if other conditions permit, any cycle in P may peak (and trough) likewise, *between* springs and neaps. In fact, the interaction of certain temporal patterns in k_{PAR} with a tidally varying water depth can also produce surprising cycles in P, without apparent regard to S_2 phase. It is therefore advisable to first probe the nature of any cycle by applying Tool 1 to several days throughout a springs–neaps cycle, or by constructing a numerical model, before concluding that the cycle peaks *precisely* at springs or at neaps. If necessary, Tool 2 can be adapted easily to determine the ratio of P on any two days (not just days at springs and neaps).

3.4.3. Tool 3: criteria for a seasonal switch in dominance

A graphical tool for predicting seasonal switches in the sense of springs–neaps cycles in P can be produced by plotting $D_{S/N}$ (calculated by Eq. (7)) against daylength, L, for different combinations of daily mean turbidity, tidal range, and times of low water, at springs and neaps. It is difficult, however, to obtain a clear, universal tool given the large number of permutations to explore and curves to plot.

The exercise was simplified somewhat by producing two separate figures for two distinct cases. Fig. 11 applies to locations with an S_2 phase of 0°, such as the Menai Strait. Thus, times of low water were set to about midday and midnight at neaps, and 6 am and 6 pm at springs. Fig. 12 applies to locations with an S_2 phase of 180°, for example the Bay of Brest. Times of low water were set, therefore, to about midday and midnight at springs, 6 am and 6 pm at neaps. This approach is not universal – there are other possible S_2 phases – but such tools provide conceptual understanding and may help to indicate sites that should be probed further for signs of a seasonal switch.

The task was simplified further by selecting an arbitrary but sensible value of daily mean attenuation coefficient and of tidal range to

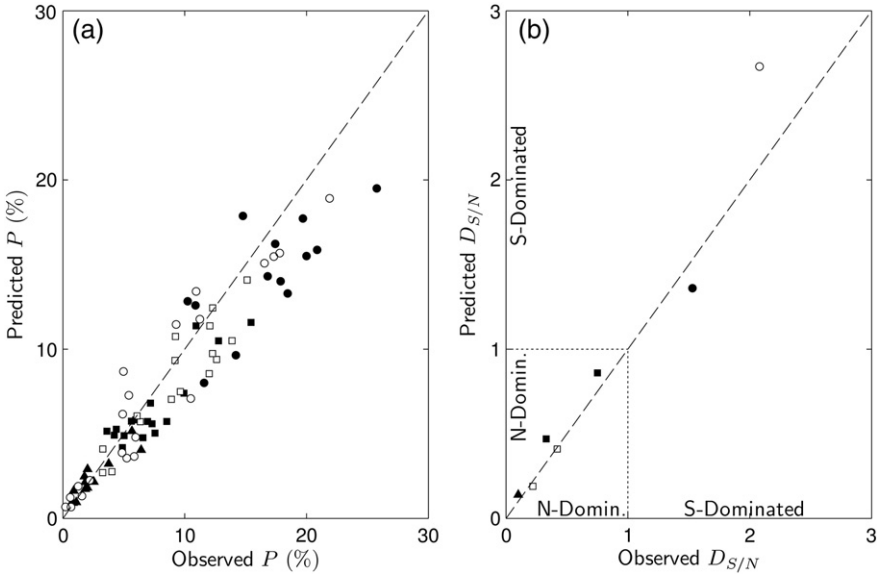

Fig. 10. Plot of: (a) the percentage of daily total sea surface irradiance received by the seabed, P, predicted by Analytical Tool 1 (Eq. (6)), against the observed values; and (b) springs–neaps dominance ratios, $D_{S/N}$, predicted by Analytical Tool 2 (Eq. (7)), against observed values. Five separate data sets were used to test the analytical tools: Menai Strait January (▲), June (■) and August (□) 2011; and Bay of Brest July (●) and December (○) 2011. Each 'observed' $D_{S/N}$ value was determined as the ratio of P from a day at spring tides to P from a day at an adjacent neaps. The five datasets provided seven such values. The dashed lines in both plots represent 1:1 lines of perfect agreement. The additional dotted lines in (b) denote $D_{S/N} = 1$, the threshold separating springs-dominated from neaps-dominated cycles in P. Note that the Menai Strait cycles are neap-dominated, whilst the Brest cycles are springs-dominated.

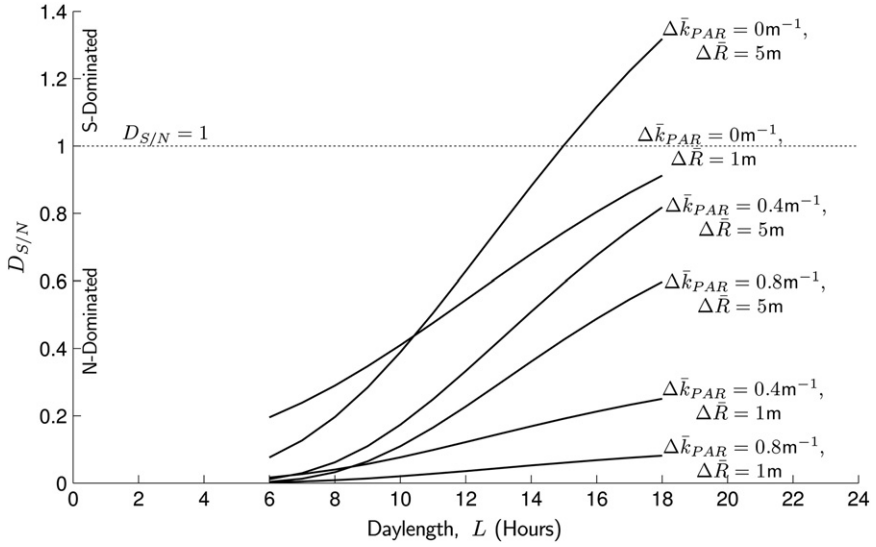

Fig. 11. Springs–neaps dominance ratio, $D_{S/N}$, plotted against daylength, L, for a hypothetical location with an S_2 phase of 0°. Six curves are plotted, each representing a different scenario whereby springs and neaps differ in terms of daily mean attenuation coefficient and tidal range. A large, moderate, and no difference in attenuation coefficient ($\Delta\bar{k}_{PAR}$) were each combined with a large and a small difference in tidal range ($\Delta\bar{R}$) to create the six scenarios. The mean water depth, z_0, was set to 4 m, so each curve represents a shallow, sub-tidal scenario. The intersection of a curve with the dashed $D_{S/N} = 1$ line indicates a switch from a neaps-dominated to a springs-dominated regime, or vice versa.

represent a typical neap tide (i.e., $\bar{k}_{PAR,N} = 0.4\text{m}^{-1}$ and $\bar{R}_N = 2.5\text{m}$). A number of different attenuation coefficients and tidal ranges were then chosen to represent hypothetical spring tide conditions (i.e., $\bar{k}_{PAR,S}$ and $\bar{R}_S$). Essentially, neap tide conditions were held constant and a number of scenarios of relative difference between springs and neaps were created by the use of different values of turbidity and tidal range at springs only. $\bar{k}_{PAR,S}$ values were selected to give a large, moderate or no difference between springs and neaps (i.e., $\Delta\bar{k}_{PAR}$). $\bar{R}_S$ values were selected to give a large or a small difference in tidal range (i.e., $\Delta\bar{R}$) between springs and neaps. The three $\Delta\bar{k}_{PAR}$ (large, moderate and zero) and two $\Delta\bar{R}$ (large and small) conditions were combined in all possible permutations to create six separate scenarios. Thus, six $D_{S/N}$ curves are plotted on each figure. Note that in choosing spring tide values, it was assumed that $\bar{k}_{PAR,S} \geq \bar{k}_{PAR,N}$ and $\bar{R}_S > \bar{R}_N$. In each scenario, springs and neaps $\bar{k}_{PAR}$ and $\bar{R}$ values were kept constant throughout the year.

The mean water depth, z_0, was set to 4 m. Given that the largest tidal amplitude considered was 3.75 m, each curve represents the case at a seabed site that is always fully immersed and is located within the shallow sub-tidal zone.

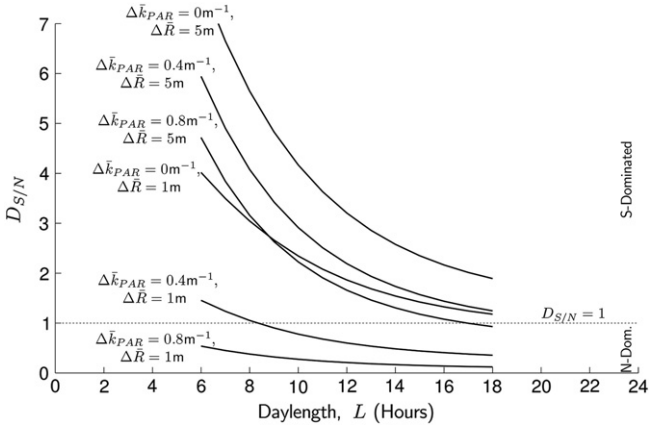

Fig. 12. Springs–neaps dominance ratio, $D_{S/N}$, plotted against daylength, L, for a hypothetical location with an S_2 phase of 180°. Six curves are plotted, each representing a different scenario whereby springs and neaps differ in terms of daily mean attenuation coefficient and tidal range. That is, three $\Delta\bar{k}_{PAR}$ values were combined with two $\Delta\bar{R}$ values in all possible permutations, as explained in Fig. 11. The mean water depth, z_0, was again set to 4 m, giving shallow, sub-tidal scenarios. Intersection of a curve with the dashed $D_{S/N} = 1$ line indicates a switch from a neaps-dominated to a springs-dominated regime, or vice versa.

In Figs. 11 and 12, a switch is predicted if a curve intersects the dashed line $D_{S/N} = 1$. For an S_2 phase of 0° (Fig. 11), a switch occurs, or nearly occurs, in cases where spring tides are not much more turbid than neaps (i.e., $\Delta\bar{k}_{PAR}$ is small), or they have a much larger tidal range (with much lower low waters) than neaps (i.e., $\Delta\bar{R}$ is large), or both. This makes physical sense; if the cycle in P is to switch from neaps-dominated in the winter to springs-dominated in the summer the morning and evening low water springs must be able to contribute significantly to P_S as daylength increases. They can only do so, and P_S can only surpass P_N as summer arrives, if spring tides are not much more turbid, or they have a much larger tidal range, or both. In the case of the curve displaying a clear switch in Fig. 11 (labelled $\Delta\bar{k}_{PAR} = 0\text{m}^{-1}$, $\Delta\bar{R} = 5\text{m}$), both preconditions are met. Where they are not met the tendency is for a neaps-dominated cycle in P throughout the year.

For an S_2 phase of 180° (Fig. 12), the tendency is for any cycle in P to be springs-dominated in the winter and, indeed, throughout the year; a low water of spring tides always coincides with the sea surface irradiance maximum at midday. In this case, it is the low waters of neaps tides, occurring at about 6 am and 6 pm, that must contribute more substantially to P_N as the days lengthen if the cycle is to switch to neaps-dominated in the summer. The preconditions for such a switch are that neaps must be less turbid than springs (i.e., $\Delta\bar{k}_{PAR}$ is moderate to large), and the tidal range at neaps must be similar to that at springs (i.e., $\Delta\bar{R}$ is small). In the scenario represented by the curve labelled $\Delta\bar{k}_{PAR} = 0.4\text{m}^{-1}$, $\Delta\bar{R} = 1\text{m}$ in Fig. 12, these preconditions are met satisfactorily, and a switch occurs.

A useful mathematical tool for indicating the *possibility* of a switch is provided by the factor (or multiplier) α_S/α_N from the analytical equation for $D_{S/N}$ (Eq. (7)). We restate α_S/α_N, in terms of familiar parameters, as

$$\frac{\alpha_S}{\alpha_N} = \exp\left[\frac{(\bar{k}_{PAR,S}\bar{R}_S - \bar{k}_{PAR,N}\bar{R}_N)}{2} - z_0\Delta\bar{k}_{PAR}\right]. \quad (8)$$

For locations with a given S_2 phase, the product of the remaining factors in Eq. (7), which we shall refer to as the multiplicand, varies with daylength in a consistent, characteristic way, regardless of any

differences in other parameters. Thus, it appears that the multiplier α_S/α_N is the determining factor in whether or not a seasonal switch occurs.

For example, for locations with an S_2 phase of 0° the multiplicand always increases from almost 0 to a value less than 1 as daylength increases. Consequently, if $D_{S/N}$ is to exceed 1 in summer, and the switch to springs-dominance is to occur, we have the minimum requirement that the multiplier $\alpha_S/\alpha_N > 1$. This is only a minimum requirement, however, and typically $\alpha_S/\alpha_N \gtrsim 2$ to 3 is required for the switch to occur.

For locations with an S_2 phase of 180°, the multiplicand varies from a value greater than 1 (often substantially so) in winter to a value between about 0.3 and 1 in summer. Consequently, a multiplier value of $\alpha_S/\alpha_N \lesssim 1$ gives a good chance of a switch from springs-dominance in winter to neaps-dominance in summer. $\alpha_S/\alpha_N \lesssim 2$ to 3 may suffice in some cases. Values greater than 3 to 4, however, will tend to result in a springs-dominated cycle throughout the year, as $D_{S/N}$ cannot fall below 1. As a caveat, very small values (i.e., $\alpha_S/\alpha_N \ll 1$) can result in a neaps-dominated cycle throughout the year.

α_S/α_N (Eq. (8)) exhibits a dependence on z_0, except for the case where $\Delta\bar{k}_{PAR} = 0\ \mathrm{m}^{-1}$. In fact, α_S/α_N increases exponentially with the term $1/2(\bar{k}_{PAR,S}\bar{R}_S - \bar{k}_{PAR,N}\bar{R}_N)$ and decreases exponentially with the term $z_0\Delta\bar{k}_{PAR}$. The latter term is revealing; it dictates that *the switches discussed in this paper are essentially a shallow subtidal phenomenon*. Very large mean water depths will result in α_S/α_N values very much less than 1. Thus, the tendency will be for a neaps-dominated cycle in P throughout the year, regardless of S_2 phase. The effects of differences in tidal range between springs and neaps are effectively rendered negligible by deep water columns, and differences in turbidity become relatively more important.

α_S/α_N should be used as a guide to the possibility of a switch only. If indicated, its existence should be probed further: by applying Analytical Tools 1 (Eq. (6)) or 2 (Eq. (7)) in winter and summer; by building a numerical model (like that in Section 3.3) for the site in question; and, preferably, by making some seasonal observations.

4. Discussion

The objective of this paper was to test the hypothesis, arising from the work of Bowers et al. (1997), that a springs–neaps cycle exists in the percentage of daily total sea surface irradiance reaching the bed of the Menai Strait, P, and that the sense of this cycle 'switches' from neaps-dominated in the winter to springs-dominated in the summer. Our observations indicate that a neaps-dominated cycle is present throughout the year, and hence no such switch occurs.

The question, then, is why not? We used our data to study the temporal behaviour of turbidity and to investigate the validity of the assumption, applied in the numerical model of Bowers et al. (1997), that the diffuse attenuation coefficient of PAR, k_{PAR}, is constant over time. In fact, it varies on tidal timescales with water depth and on springs–neaps timescales with tidal range, rendering the assumption invalid. A simple, semi-empirical attempt was made to model this temporal variability of k_{PAR} mathematically. Using this to update the Bowers et al. (1997) numerical model, the switch is no longer produced. Thus, failure to account adequately for cyclical behaviour in turbidity is implicated as the likely cause of the spurious prediction of a switch. This is in agreement with the work of Desmit et al. (2005), which similarly highlights the perils of neglecting the effect of tidal SPM dynamics on turbidity when modelling the light available for primary production. A knowledge of site- and season-specific k_{PAR} variability is essential in order to accurately predict the nature of cycles in P.

We aimed to extend the work by investigating the conditions under which a switch *does actually* occur or, conversely, the conditions under which a site might experience a springs-dominated or neaps-dominated cycle throughout the year. A three tier analytical/graphical approach was adopted. Firstly, an analytical equation for P on any given day was determined. Then, by defining the ratio of this percentage at springs to that at neaps, in terms of the first analytical equation, a second equation was derived for a parameter we termed the 'springs–neaps dominance ratio', $D_{S/N}$, where $D_{S/N} < 1$ indicates a neaps-dominated cycle and $D_{S/N} > 1$ indicates a springs-dominated cycle. Finally, we explored changes in $D_{S/N}$ with daylength, L, to identify the approximate criteria for a switch, or the lack of one. Several key findings emerged:

1. Springs–neaps cycles in P are common: P is a complicated function of turbidity, tidal range, times of low water, daylength, mean water depth, and angular frequency of the tide. Inequality of P at springs and neaps (i.e., $D_{S/N} \neq 1$) is more likely than equality, and springs–neaps cycles in P are likely to be commonplace at many coastal sites.
2. For a site with an S_2 phase of 0° (i.e., low water neaps at about midday and midnight; low water springs at about 6 am and 6 pm), *the tendency is for a neaps-dominated cycle in P*. However, a switch to springs-dominated may occur as daylength increases, and the springs low waters occur within daylight hours, if the spring tides are not significantly more turbid than neaps and/or they have a substantially greater tidal range (in particular, lower low waters).
3. Conversely, for a site with an S_2 phase of 180° (i.e., low water springs at about midday and midnight; low water neaps at about 6 am and 6 pm), *the tendency is for a springs-dominated cycle in P*. A switch to a neaps-dominated cycle may occur as daylength increases, and the neaps low waters occur within daylight hours, if spring tides are typically much more turbid than neaps and/or there is little difference in tidal range.
4. α_S/α_N is a key parameter for determining the possibility of a switch. It can be used to indicate the need for further investigation with analytical tools and numerical models, such as those developed in this paper, or with observations.
5. Switches are essentially a shallow, sub-tidal phenomenon: α_S/α_N decreases exponentially with the term $z_0\Delta\bar{k}_{PAR}$. For $\bar{k}_{PAR,S} > \bar{k}_{PAR,N}$ (i.e., $\Delta\bar{k}_{PAR} > 0\ \mathrm{m}^{-1}$), a large mean water depth will result in a small α_S/α_N value, and thus a small $D_{S/N}$ throughout the year. That is to say, any cycle in P at relatively large mean depths will tend to remain neaps-dominated, and no switch will occur.

There are a number of limitations associated with the work in this paper. Firstly, observations were made at only two sites with two different S_2 phases (focus being on Menai Strait data in this paper, with Bay of Brest data used only to test the analytical tools). Biofouling and weather/hydrodynamic conditions meant that the time series obtained were constrained to just 1–2 springs–neaps cycles at a time. Despite this, the patterns observed are sufficiently clear to suspect a strong underlying physical mechanism with a repeating nature. Several additional irradiance datasets, not shown in this paper, exhibit similar springs–neaps patterns, and other authors report likewise for different sites: Topliss (1977) (North Wales); Pilgrim and Millward (1989) (Tamar Estuary, southern England); and, notably, Dring and Lüning (1994) (southern North Sea).

Secondly, August 2011 data was used to explore the temporal variability of k_{PAR} in the Menai Strait. The resulting semi-empirical equation describing the variability was used to update the numerical model of Bowers et al. (1997). As noted already, the temporal behaviour of k_{PAR} is likely to be strongly site- and season-specific, and so the approach adopted here should be considered demonstrative only. Our k_{PAR} equation should not be applied when modelling other locations and, in fact, its derivation from summer data is probably responsible for the updated model overestimating the amplitude of the P cycle in winter for the Menai Strait.

Thirdly, in attempting to model k_{PAR} variability, two distinct physical mechanisms were proposed: a $\bar{k}_{PAR}$ dependence on tidal range, $\bar{R}$; and a k_{PAR} dependence on water depth, z. Whilst both are feasible, the latter effect could be partially or wholly responsible for the former. Times of low water advance; the portion of any tidal cycle in turbidity (more explicitly, the number peaks and troughs) occurring within daylight hours varies over the springs–neaps cycle. This will exert a control on the calculated daily mean attenuation coefficient, $\bar{k}_{PAR}$,

meaning that apparent changes in this parameter with $\overline{R}$ may be as much a consequence of k_{PAR}'s dependence on z as of an independent physical mechanism. Substantiating and resolving these mechanisms may provide an interesting task for future research.

The remaining limitations arise from the use of daily mean attenuation coefficients to make the analytical equations possible. k_{PAR} has been shown in this paper to vary in regular ways *during* the day (with the tide), and this is not accounted for by the use of daily mean values. Despite this, and the additional limitations introduced by the use of the simplifying assumptions of Bowers and Brubaker (2010), the equations perform encouragingly well for the Menai Strait and Bay of Brest. Discrepancies between predictions and observations are small and typically due to the aforementioned tidal variability in k_{PAR} and to intermittent cloud cover, both of which affect the observations but are unaccounted for by the equations. The graphical tools (Figs. 11 and 12) are produced on the premise that $\overline{k}_{PAR,S}$ and $\overline{k}_{PAR,N}$ are constant at a given site throughout the year, or more specifically that their difference does not change. This is unlikely to be the case, but the broad physical understanding that the figures provide should remain valid. Ultimately, the tools must be tested against observations from other sites in future.

The implications of this work are mostly ecological. Throughout, we have normalised the daily total seabed irradiance, $\langle I_B \rangle$, by the daily total sea surface irradiance, $\langle I_0 \rangle$. This removes some of the noise in the springs–neaps patterns introduced by variability in $\langle I_0 \rangle$ from day-to-day, owing to differences in atmospheric conditions. However, it is reasonable to expect springs–neaps patterns to be present in the non-normalised parameter $\langle I_B \rangle$, on average (over a few cycles). Consequently, we might also expect light-limited benthic algae (and plants) growing at shallow, sub-tidal sites to exhibit corresponding springs–neaps patterns in daily total primary production.

Caution must be applied when making such assertions; many benthic algae are 'shade-adapted', and their photosynthesis may be saturated, or even inhibited, at relatively low light levels. Large values of $\langle I_B \rangle$ resulting from strong peaks in seabed irradiance may not, therefore, translate directly into particularly large daily total production if photosynthesis is saturated or inhibited for long periods of the day. The brown and red algae occupying the shallow sub-tidal zone require irradiances of just 150–250 μmol quanta m^{-2} s^{-1} to saturate photosynthesis (Lüning, 1981). For the common, shallow sub-tidal kelp *Saccharina latissima*, saturation irradiances of 100–150 μmol quanta m^{-2} s^{-1} have been reported (Gévaert et al., 2002; Lüning, 1979), whereas for the red alga *Chondrus crispus* the literature values are a little higher at 120–260 μmol quanta m^{-2} s^{-1} (Lüning, 1981; Mathieson and Norall, 1975). Given that winter seabed irradiances observed in the current study (at a mean depth of about 4 m in the Menai Strait) did not exceed 100 μmol quanta m^{-2} s^{-1}, photosynthesis in hypothetical specimens of these two example species, growing at that depth, should have responded linearly to irradiance throughout the observation period. Under such conditions, it follows that any pattern in $\langle I_B \rangle$ be mirrored by a pattern in daily total primary production. This may be of particular importance in the case of the genus *Laminaria*, which exhibits a fast growth period in the winter and spring (Dring, 1992; Kain, 1979).

In the summer, the situation is not so clear; observed irradiances occasionally reached 500 μmol quanta m^{-2} s^{-1}, sufficient to saturate photosynthesis and even cause photoinhibition in our example species (based on photosynthesis parameters reported in Mathieson and Norall (1975) and Gévaert et al. (2003)). It is difficult to gain an intuitive understanding of how daily total primary production might respond in this case, without in-situ measurements. The same is true if we are considering our two example species growing at shallower (and brighter) depths, or we are considering different species with lower saturation irradiances (e.g., deeper-water red algae are often light-saturated at just 60–70 μmol quanta m^{-2} s^{-1} (Dring, 1992)). Here, again, saturation and photoinhibition are potentially prevalent. Some insight into the relative benefits of particular phases of the springs–neaps cycle to a specimen of benthic algae may be obtained by inputting seabed irradiance time series into a photosynthesis–irradiance equation (e.g., the equations of Webb et al. (1974), Jassby and Platt (1976), and Peeters and Eilers (1978)), in a manner akin to that presented by Zimmerman et al. (1994). This approach is undertaken in a forthcoming paper.

In terms of practical applications, our findings are potentially of use to habitat managers and policy makers involved in the protection or re-colonisation of macroalgal (and angiospermous) beds. One phase of the springs–neaps tidal cycle may be more advantageous than others, in terms of irradiance and photosynthesis at the seabed. It may be necessary to legislate to protect this phase above others, perhaps by ensuring effluents are not permitted to cause a decline in water clarity at key times. Re-introduction schemes may look to exploit a potential site on the basis of a favourable springs–neaps cycle in P. In both cases, constructing a numerical model or using the analytical tools, developed in this paper, for the site in question is recommended.

Our analytical tools and conclusions are applicable to locations where the tidal regime is semi-diurnal, with M_2 and S_2 tidal constituents dominating. Whilst this regime is the most common (Pugh, 1996), there are locations where diurnal tidal constituents, particularly the luni-solar diurnal (K_1) and principal lunar diurnal (O_1), are larger in amplitude than the S_2, or even both the S_2 and M_2. The result is (respectively) a mixed tidal regime (e.g., parts of the Persian Gulf, the Philippines, and the west coast of the United States) or a diurnal tidal regime (e.g., the Gulf of Mexico, the Gulf of Carpentaria in Australia, and parts of the Persian Gulf and South China Sea) (Boon, 2004; Pugh, 1996). Adapting our tools for such locations was beyond the scope of this paper. However, diurnal tides in particular present interesting questions in light of the current work. Their range varies with a semi-monthly periodicity, driven by the lunar declination cycle; the terms 'diurnal springs' and 'diurnal neaps' have even been proposed to describe the phenomenon (Doodson and Warburg, 1941). The times of low and high waters also shift from day to day, though they do not continuously advance as with semi-diurnal tides. It therefore seems likely that regular patterns in P will be observed for diurnal tides. These have the potential to be quite pronounced. However, they are likely to be less susceptible to the seasonal, daylength-induced 'switches of sense' described in this paper, which are perhaps impossible for all but the highest latitude (diurnal regime) sites experiencing the greatest daylength variation.

Acknowledgements

This work was supported by the Natural Environment Research Council [Grant Number NE/I527853/1]. Many thanks to Gwynne Parry Jones, Ben Powell and Pete Hughes, for facilitating the fieldwork in North Wales, and to Georges Chapalain, Alexis Beudin and Antoine Douchin, for enabling two deployments in Brittany. Special thanks to Ian Nicholls, for fabricating innovative and robust deployment materials, Geraint Roberts, for casting a critical eye over the manuscript, and Malen Jukes, for invaluable discussions and steadfast encouragement. The authors are grateful to three anonymous reviewers of this manuscript for their helpful suggestions.

References

Anthony, K.R.N., Ridd, P.V., Orpin, A.R., Larcombe, P., Lough, J., 2004. Temporal variation of light availability in coastal benthic habitats: effects of clouds, turbidity, and tides. Limnol. Oceanogr. 49, 2201–2211.

Bassoullet, P., 1979. Étude des sédiments en suspension dans l'estuaire de l'Aulne. (Ph.d. thesis) Université de Bretagne Occidentale, Brest.

Boon, J.D., 2004. Secrets of the Tide. Horwood Publishing Limited, Chichester.

Bowers, D.G., 2003. A simple turbulent energy-based model of fine suspended sediments in the Irish Sea. Cont. Shelf Res. 23, 1495–1505.

Bowers, D.G., Brubaker, J.M., 2004. Underwater sunlight maxima in the Menai Strait. J. Opt. A Pure Appl. Opt. 6, 684–689.

Bowers, D.G., Brubaker, J.M., 2010. Tidal amplification of seabed light. J. Geophys. Res. 115, C09008.

Bowers, D.G., Tett, P., Walne, A.W., 1997. A note on seabed irradiance in shallow tidal seas. J. Mar. Biol. Assoc. U. K. 77, 921–928.

Buchan, S., Floodgate, G.D., Crisp, D.J., 1967. Studies on the seasonal variation of the suspended matter in the Menai Straits. I. The inorganic fraction. Limnol. Oceanogr. 12, 419–432.
Carter, V., Rybicki, N.B., 1990. Light attenuation and submersed macrophyte distribution in the tidal Potomac River and Estuary. Estuaries 13, 441–452.
Delmas, R., 1981. Étude de l'évolution saisonnière des sels nutritifs dans la rade de Brest en fonction des apports fluviaux et des échanges avec l'Iroise. (Ph.d. thesis) Université de Bretagne Occidentale, Brest.
Delmas, R., Tréguer, P., 1983. Évolution saisonnière des nutriments dans un écosystème eutrophe d'Europe Occidentale (la rade de Brest). Interactions marines et terrestres. Oceanol. Acta 6, 345–355.
Dennison, W.C., 1987. Effects of light on seagrass photosynthesis, growth and depth distribution. Aquat. Bot. 27, 15–26.
Desmit, X., Vanderborght, J.P., Regnier, P., Wollast, R., 2005. Control of phytoplankton production by physical forcing in a strongly tidal, well-mixed estuary. Biogeosciences 2, 205–218.
Doodson, A.T., Warburg, H.D., 1941. Admiralty Manual of Tides. HMSO, London.
Dring, M.J., 1987. Light climate in intertidal and subtidal zones in relation to photosynthesis and growth of benthic algae: a theoretical model. In: Crawford, R.M.M. (Ed.), Plant Life in Aquatic and Amphibious Habitats. Blackwell, Oxford, pp. 23–34.
Dring, M.J., 1992. The Biology of Marine Plants. Cambridge University Press, Cambridge.
Dring, M.J., Lüning, K., 1994. Influence of springs–neaps tidal cycles on the light available for photosynthesis by benthic marine plants. Mar. Ecol. Prog. Ser. 104, 131–137.
Duarte, C.M., 1991. Seagrass depth limits. Aquat. Bot. 40, 363–377.
Embleton, C., 1964. The deglaciation of Arfon and southern Anglesey, and the origin of the Menai Straits. Proc. Geol. Assoc. 75, 407–429.
Gévaert, F., Créach, A., Davoult, D., Holl, A.C., Seuront, L., Lemoine, Y., 2002. Photoinhibition and seasonal photosynthetic performance of the seaweed Laminaria saccharina during a simulated tidal cycle: chlorophyll fluorescence measurements and pigment analysis. Plant Cell Environ. 25, 859–872.
Gévaert, F., Créach, A., Davoult, D., Migné, A., Levavasseur, G., Arzel, P., Holl, A.C., Lemoine, Y., 2003. Laminaria saccharina photosynthesis measured in situ: photoinhibition and xanthophyll cycle during a tidal cycle. Mar. Ecol. Prog. Ser. 247, 43–50.
Harvey, J.G., 1968. The flow of water through the Menai Straits. Geophys. J. R. Astron. Soc. 15, 517–528.
Jassby, A.D., Platt, T., 1976. Mathematical formulation of the relationship between photosynthesis and light for phytoplankton. Limnol. Oceanogr. 21, 540–547.
Kain, J.M., 1979. A view of the genus Laminaria. Oceanogr. Mar. Biol. Annu. Rev. 17, 101–161.
Kirk, J.T.O., 1994. Light and Photosynthesis in Aquatic Ecosystems, second ed. Cambridge University Press, Cambridge.
Koch, E.W., Beer, S., 1996. Tides, light and the distribution of Zostera marina in Long Island Sound, USA. Aquat. Bot. 53, 97–107.
Kratzer, S., Buchan, S., Bowers, D.G., 2003. Testing long-term trends in turbidity in the Menai Strait, North Wales. Estuar. Coast. Shelf Sci. 56, 221–226.
L'Yavanc, J., 1984. Étude hydrologique de l'estuaire de l'Élorn. Rapport IFREMER-DERO/EL. Technical Report. IFREMER, Plouzané.
Le Pape, O., 1997. Modélisation du cycle biogéochimique des éléments limitant la production primaire en rade de Brest. (Ph.d. thesis) Ecole Nationale Supérieure Agronomique de Rennes.
Lobban, C.S., Harrison, P.J., 1997. Seaweed Ecology and Physiology. Cambridge University Press, Cambridge.
Lüning, K., 1979. Growth strategies of three Laminaria species (Phaeophyceae) inhabiting different depth zones in the sublittoral region of Helgoland (North Sea). Mar. Ecol. Prog. Ser. 1, 195–207.
Lüning, K., 1981. Light. In: Lobban, C.S., Wynne, M.J. (Eds.), The Biology of Seaweeds. Blackwell, Oxford, pp. 326–355.
Mathieson, A.C., Norall, T.L., 1975. Photosynthetic studies of Chondrus crispus. Mar. Biol. 33, 207–213.
Monbet, Y., Bassoullet, P., 1989. Bilan des connaissances océanographiques en rade de Brest. Rapport CEA/IPSN, code DERO/EL 89-23, IFREMER-DEL-BP 70-29280. Technical Report. IFREMER, Plouzané.
Peeters, J.C.H., Eilers, P., 1978. The relationship between light intensity and photosynthesis — a simple mathematical model. Hydrobiol. Bull. 12, 134–136.
Pilgrim, D.A., Millward, G.E., 1989. Variation in the diffuse optical depth of the bed of a tidal estuary. In: McManus, J., Elliott, M. (Eds.), Developments in Estuarine and Coastal Study Techniques. Olsen and Olsen, Fredensborg, pp. 101–107.
Pingree, R.D., Griffiths, D.K., 1981. S2 tidal simulations on the north-west European shelf. J. Mar. Biol. Assoc. U. K. 61, 609–616.
Pugh, D.T., 1996. Tides, Surges, and Mean Sea-Level. John Wiley and Sons, Chichester.
Salomon, J.C., Breton, M., 1991. Numerical study of the dispersive capacity of the Bay of Brest, France, towards dissolved substances. In: Lee, J.H.W., Cheung, Y.K. (Eds.), Environmental Hydraulics. Balkema, Rotterdam, pp. 459–464.
Thouzeau, G., Chauvaud, L., Grall, J., Guérin, L., 2000. Rôle des interactions biotiques sur le devenir du pré-recrutement et la croissance de Pecten maximus (L.) en rade de Brest. C. R. Acad. Sci. III Sci. Vie 323, 815–825.
Topliss, B.J., 1977. A Study of Optical Irradiance in Coastal Waters. (Ph.d. thesis) University of Wales, Bangor.
Topliss, B.J., Hunter, J.R., Simpson, J.H., 1980. Simultaneous measurements of transparency and irradiance in the coastal waters of North Wales. Mar. Environ. Res. 4, 65–79.
Vant, W.N., Davies-Colley, R.J., Clayton, J.S., Coffey, B.T., 1986. Macrophyte depth limits in North Island (New Zealand) lakes of differing clarity. Hydrobiologia 137, 55–60.
Webb, W.L., Newton, M., Starr, D., 1974. Carbon dioxide exchange of Alnus rubra: a mathematical model. Oecologia 17, 281–291.
Zimmerman, R.C., Cabello-Pasini, A., Alberte, R.S., 1994. Modeling daily production of aquatic macrophytes from irradiance measurements: a comparative analysis. Mar. Ecol. Prog. Ser. 114, 185–196.